Structural, electronic and magnetic properties of cementite-type Fe3X (X=B, C, N) by first-principles calculations

ARTICLE *in* SOLID STATE SCIENCES · MARCH 2010

Impact Factor: 1.84 · DOI: 10.1016/j.solidstatesciences.2009.12.004

6 AUTHORS, INCLUDING:

Zhiqing Lv
Yan Shan University
31 PUBLICATIONS **246** CITATIONS
SEE PROFILE

Wan-tang Fu
Yan Shan University
55 PUBLICATIONS **374** CITATIONS
SEE PROFILE

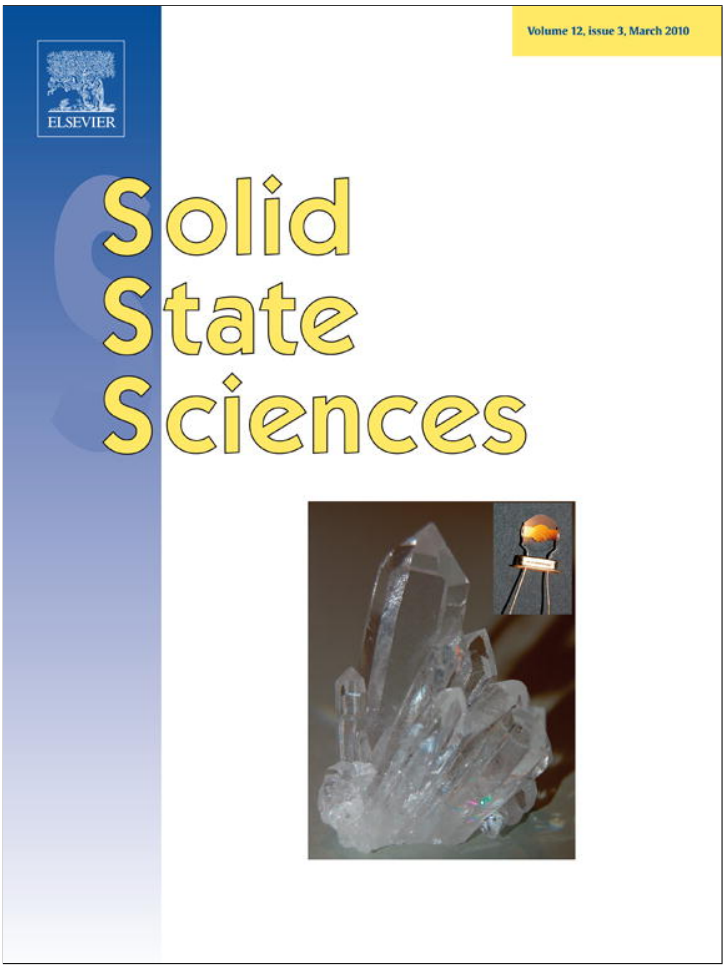

Solid State Sciences 12 (2010) 404–408

Contents lists available at ScienceDirect

Solid State Sciences

journal homepage: www.elsevier.com/locate/ssscie

Structural, electronic and magnetic properties of cementite-type Fe_3X (X = B, C, N) by first-principles calculations☆

Z.Q. Lv[a,b], W.T. Fu[a,*], S.H. Sun[a,c], Z.H. Wang[a], W. Fan[a], M.G. Qv[a]

[a] State Key Laboratory of Metastable Material Science and Technology, Yanshan University, Qinhuangdao 066004, China
[b] College of Mechanical Engineering, Yanshan University, Qinhuangdao 066004, China
[c] College of Science, Yanshan University, Qinhuangdao 066004, China

ARTICLE INFO

Article history:
Received 6 August 2009
Received in revised form
18 November 2009
Accepted 3 December 2009
Available online 11 December 2009

Keywords:
Electronic structure
Magnetic properties
First-principles
Cementite
Crystal structure

ABSTRACT

Using first-principles technique, the crystal structure of cementite-type Fe_3N is predicted. The average magnetic moment (Ms) of cementite-type Fe_3N is also predicted as 1.4929 μ_B/atom. The Ms of Fe_3N is bigger than that of Fe_3C, but smaller than that of Fe_3B. Fe Ms between two different Fe sites in Fe_3N are different (2.0541 and 2.0139 μ_B), which indicates that Fe Ms are sensitive to the local short-range order in the cementite-type crystal. The Ms of B, C and N are −0.3525, −0.2474 and −0.1102 μ_B/atom in Fe_3X (X = B, C, N), respectively. The chemical bonds of Fe_3X (X = B, C, N) take on metallicity, covalence, and ionicity. The ionicity of Fe_3X (X = B, C, N) strengthens and the covalence of Fe–X weakens, going from Fe_3B, Fe_3C to Fe_3N.

1. Introduction

As the cementite-type Fe_3X (X = B, C, N) with orthorhombic structure are the most important strengthening phases in carbon and alloy steels, the carburizing, boriding and nitriding technology are applied widely to improve the surface properties of the steels [1–3]. In some cases, Fe_3B and Fe_3N are also the important composition phases in the other ferromagnetic materials [4–6]. Although the structural, electronic, and magnetic properties of Fe_3N with hexagonal structure have been investigated [6,7], there are few reports on the properties of cementite-type Fe_3N. The investigations on the electronic structure and magnetic properties of Fe_3X (X = B, C, N) are a significant contribution to clarify the relationship between them and predict the properties of the cementite-type Fe_3N.

The present study aims to examine the electronic and magnetic properties of cementite-type Fe_3X (X = B, C, N) and to clarify the relationship between them by using the first-principles method. As a result, the crystal structural, electronic and magnetic properties of the cementite-type Fe_3N are predicted.

2. Crystal structure and calculation details

All calculations were performed for cementite-type Fe_3X (where X = B, C, N) using CASTEP code [8] based on the Density-Function Theory (DFT) [9,10]. The electron–ion interactions are described by using the Vanderbilt ultrasoft pseudopotential (USPP) [11]. The exchange and correlation terms are treated by Generalized Gradient Approximation (GGA) in the scheme of Revised Perdew–Burke–Eruzer (RPBE) [12]. It is needed to mention that the used USPP should be compatible with the special type of GGA. For the Brillouin-Zone sampling, the Monkhorst–Pack Scheme [13] was adopted.

In the calculations of Fe_3X (X = B, C, N), we used $5 \times 4 \times 6$ mesh of special k-points and the kinetic energy cutoff (E_{cut}) $E_{cut} = 500$ eV for the GGA calculations. Spin polarization is considered at each calculation. Each calculation was considered convergence when the maximum force on the atom was below 0.006 eV Å^{-1} and the maximum displacement between cycles was below 2×10^{-4} Å. The cementite-type Fe_3X (X = B, C, N) crystallize in the orthorhombic space group Pnma (SP No. 62) with four formula units ($Z = 4$) per unit cell, where four iron atoms (FeI) in "special" positions, eight

☆ This work was supported by the Natural Science Foundation of China (No. 50671089 and No. 50471102).
* Corresponding author. Tel.: +86 335 838 7472.
E-mail address: wtfu@ysu.edu.cn (W.T. Fu).

1293-2558/$ – see front matter © 2009 Elsevier Masson SAS. All rights reserved.
doi:10.1016/j.solidstatesciences.2009.12.004

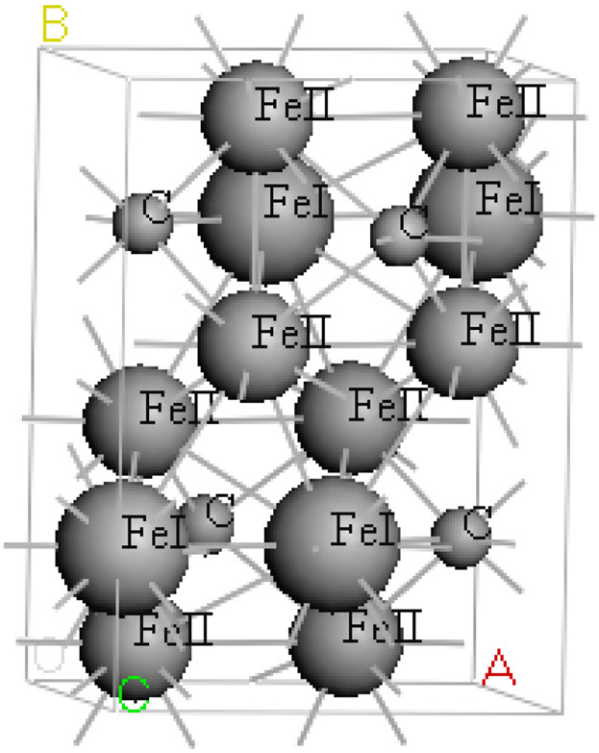

Fig. 1. Crystal structure of cementite-type Fe_3X, showing the orthorhombic space lattice and the sixteen atoms basis.

iron atoms (FeII) are in "general" positions, and four nonmetal atoms (B, C, N) in the interstices [14]. A three-dimensional drawing of the unit cell is shown in Fig. 1.

3. Results and discussions

3.1. Structural properties of cementite-type Fe_3X (X = B, C, N)

The ground state properties of the cementite-type Fe_3X (X = B, C, N) are investigated from their total energy, which is calculated as a function of volume. When it is according to the Murnaghan equation of state [15], the equilibrium lattice constants and atomic positions can be obtained (see Table 1). It can be found that the GGA values of the lattice constants match fairly well with the experimental ones for Fe_3B [16] and Fe_3C [17]. The deviations between the experimental and theoretical values of cell volume are 0.32% and 0.28% for Fe_3B and Fe_3C, respectively. Based on the same method the crystal structure of the cementite-type Fe_3N is predicted (shown in Table 1).

Table 1
Experimental and calculated lattice constants a_0, b_0, c_0 (Å), v_0 (Å^3), ρ (g/cm^3) and E_{cell} (eV) of Fe_3B, Fe_3C and Fe_3N.

	Fe_3B (Ref. [16])	Fe_3C (Ref. [17])	Fe_3N
a	5.437 (5.433)	5.053 (5.082)	4.955
b	6.710 (6.656)	6.775 (6.733)	7.124
c	4.387 (4.454)	4.504 (4.521)	4.506
Fe_I	0.02041, 0.25000, 0.88216	0.03887, 0.25000, 0.83490	0.05881, 0.25000, 0.81467
Fe_{II}	0.17557, 0.44364, 0.35267	0.17654, 0.43136, 0.33139	0.17374, 0.42347, 0.31483
X	0.38182, 0.25000, 0.07487	0.37688, 0.25000, 0.06203	0.38201, 0.25000, 0.06536
V	160.055 (161.066)	154.258 (154.696)	159.067
ρ	7.401 (7.355)	7.731 (7.709)	7.581
E_{total} (cell)	−10 706.46	−11 013.76	−11 477.78

3.2. Electronic properties of cementite-type Fe_3X (X = B, C, N)

Considering the results obtained from the electronic structure of cementite-type Fe_3X (X = B, C, N) at equilibrium, the electronic properties of them from the plots of DOSs (density of states) are discussed. The site- and spin-projected DOSs are shown in Fig. 2 for Fe_3X (X = B, C, N) at theoretical equilibrium lattice constants. It can be seen that for Fe_3X (X = B, C, N), there are three regions: the lowest valence band, the upper valence band, and the conduction

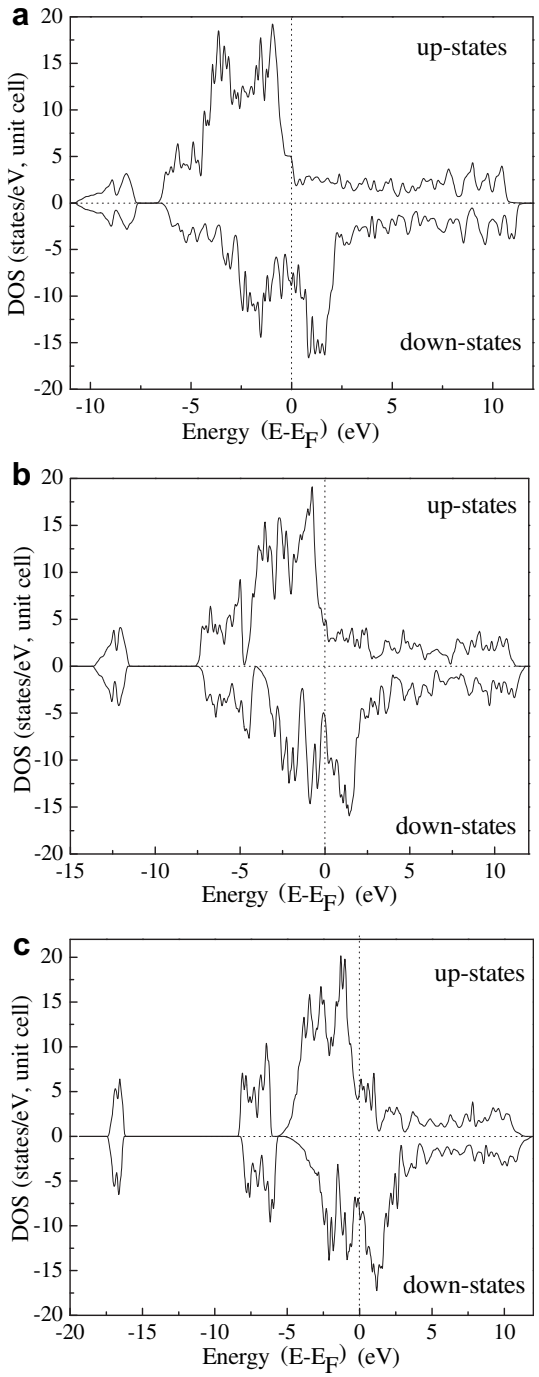

Fig. 2. Calculated spin-polarized total density of states of (a) Fe_3B, (b) Fe_3C, (c) Fe_3N.

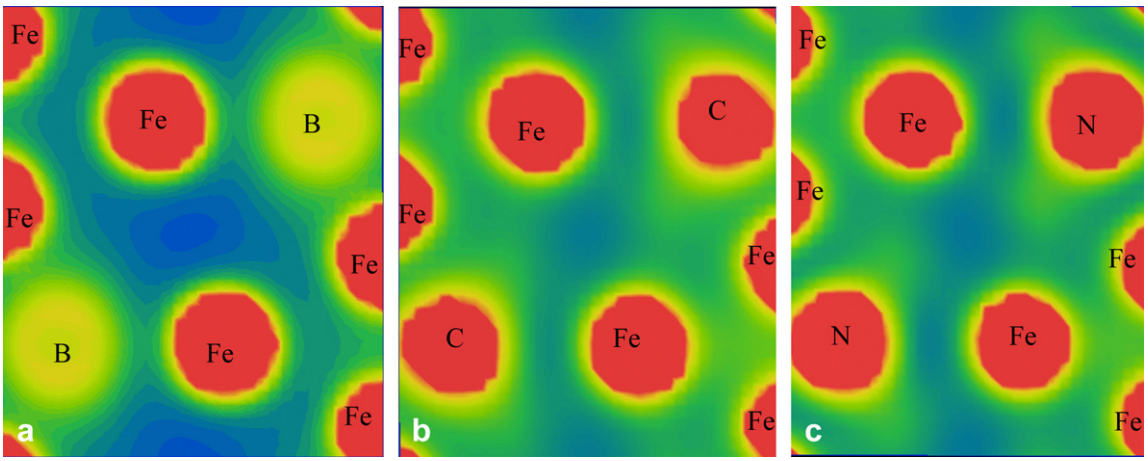

Fig. 3. Total electron density distribution map of the plane with Fe and X atoms of Fe_3X plotted from 0.01 (blue) to 1 (red) e $Å^{-3}$, electron density values larger than 1 are not shown (a) Fe_3B, (b) Fe_3C, (c) Fe_3N. (For interpretation of the references to colour in this figure legend, the read is referred to the web version of this article.)

unoccupied states. The lowest valence band ranging consists of a mixture of X (B, C, N) 2s and a small contribution from *s*, *p* and *d* states of metal atoms Fe. The upper valence band mainly constituted with the hybridization of X (B, C, N) 2p and metal atoms (Fe) 3d. Comparing the up with down densities, it can be seen that the up and down states are not symmetric for them, and Fe_3X (X = B, C, N) have magnetic characters. The magnetic characters of them are manifest in the two last parts from Fig. 2. Actually, the lowest valence band is almost symmetric, and it is near to the Fermi level that the up and down states are noticeably dissimilar for them. The energy gaps between the lowest valence band and the upper valence band are 1, 4 and 7.5 eV for cementite-type Fe_3B, Fe_3C and Fe_3N, respectively. This shows that the chemical bonds of Fe_3X (X = B, C, N) take on ionicity and the ionicity of Fe–X strengthens from Fe–B, Fe–C to Fe–N. The main reason of the ionicity of Fe–X is the difference in electro-negativity between the comprising elements (Fe and X). In addition, no energy gap near to the Fermi level can be seen, and this indicates a metallic nature of Fe_3X (X = B, C, N). The bonding characters of the constituting elements can be described as a mixture of covalent–ionic and, due to the d-resonance in the vicinity of the Fermi level, partly metallic.

In Figs. 3 and 4, the electron density distribution map of the plane with Fe and X (B, C, N) atoms is plotted in two ways, the total density map and the electron density difference map. The core regions of X (X = B, C, N) and Fe have the largest density from Fig. 3, which are mainly due to ionic core orbits. The covalent bonds of Fe–X can be found in Fig. 3, which were immersed in a metallic Fermi free electron gas. The covalence of Fe–X grows, going from Fe–N, Fe–C to Fe–B. The delocalized electron clouds represent the metallic bonds between the metal atoms and the highest energy level near the Fermi surface being occupied [18]. The electron density difference was determined as $\Delta\rho = \{\rho_{crystal} - \sum \rho_{at}\}$, where $\rho_{crystal}$ and ρ_{at} are the valence electron densities for Fe_3X (X = B, C, N) and the corresponding free atoms, respectively. It can be seen that the increment of valence electrons is concentrated on the X (X = B, C, N) atoms and the elongated contours correspond to the p-like orbits of X (X = B, C, N). In the interstitial regions, the increment of delocalized electrons is attributed to the metallic bonds. From Figs. 3 and 4, it is concluded that the chemical bonds of Fe_3X (X = B, C, N) take on metallicity and covalence, and the covalence of Fe–B is strongest and that of Fe–C is weakest in them.

The differences in electro-negativity between Fe and X result in the charge transfer in Fe_3X. For explaining the charge transfer and the ionicity of Fe–X, the Mulliken populations for Fe_3X were calculated. From the Mulliken population analysis for cementite (Fe_3C), the charges of C, Fe_I and Fe_{II} atoms distribute to −0.69,

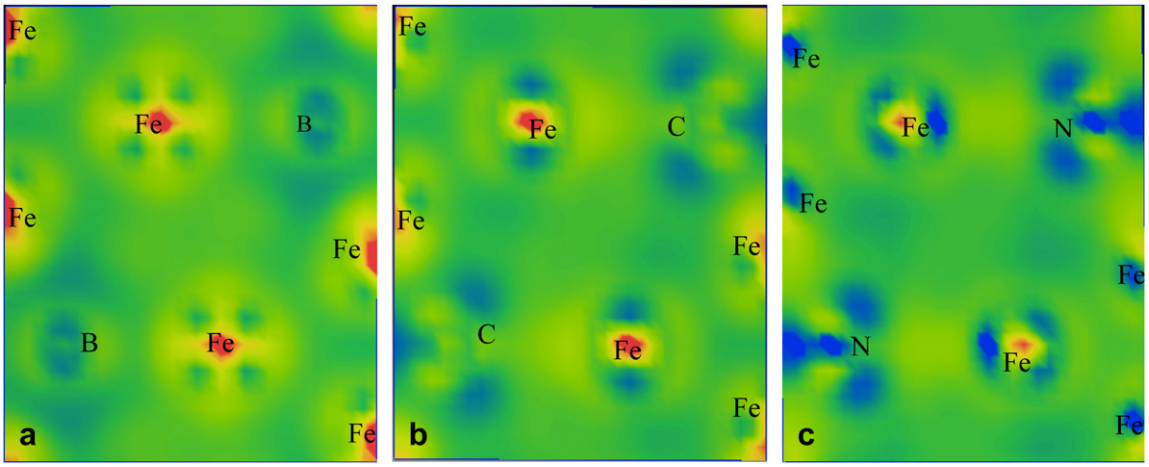

Fig. 4. Electron density difference map of the plane with Fe and X atoms of Fe_3X plotted from −0.2 (blue) to 0.1 (red) e $Å^{-3}$ (a) Fe_3B, (b) Fe_3C, (c) Fe_3N. (For interpretation of the references to colour in this figure legend, the read is referred to the web version of this article.)

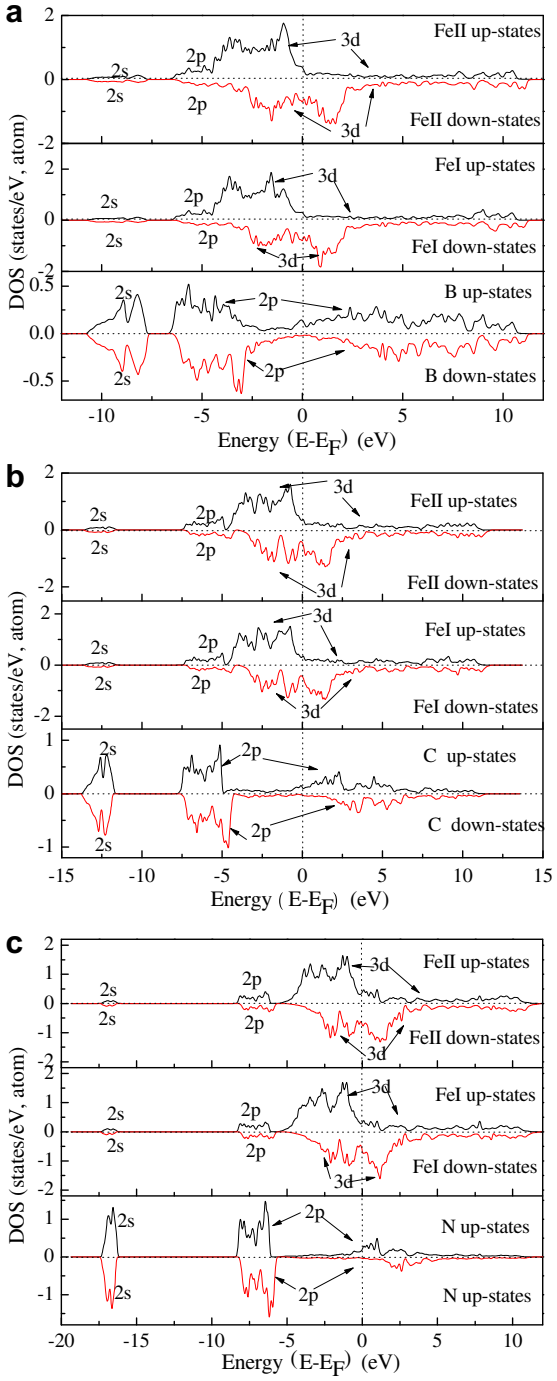

Fig. 5. Calculated site- and spin-projected partial density of states of (a) Fe_3B, (b) Fe_3C, (c) Fe_3N.

+0.19 and +0.25, respectively [19]. As for Fe_3B, the charges of B, Fe_I and Fe_{II} atoms are −0.73, +0.25 and +0.24, respectively; as for Fe_3N, the charges of N, Fe_I and Fe_{II} atoms distribute to −0.67, +0.19 and +0.24. The values of charge transfer for Fe_3C, Fe_3B and Fe_3N are 0.69, 0.73 and 0.67, respectively. The calculated lengths of the Fe–B bonds are 2.08327, 2.10503 and 2.13917 Å respectively, and the corresponding overlapping-population values are 0.35, 0.31 and 0.25 in Fe_3B. The calculated lengths of the Fe–C bonds are 1.99094, 2.00195 and 2.00849 Å respectively, and the corresponding overlapping-population values are 0.30, 0.32 and 0.34 in Fe_3C. The calculated lengths of the Fe–N bonds are 1.95992, 1.96349 and 1.97664 Å respectively, and the corresponding overlapping-population values are 0.30, 0.25 and 0.28 in Fe_3N. This indicates that the strong covalent bonding states exist in Fe_3X (X = B, C, N). The lengths of Fe–Fe bonds in Fe_3B, Fe_3C and Fe_3N are 2.45748–2.95550 Å, 2.45834–2.67174 Å and 2.47077–2.82024 Å, respectively. The variations of population values are 0.03–1, 0.06–1 and 0.03–1 in Fe_3B, Fe_3C and Fe_3N, respectively. There are no negative overlap population values of Fe–Fe bonds in Fe_3X (X = B, C, N), which indicates no repulsion force among these atoms.

Table 2
Calculated effective charges Q^*, spin magnetic moments Ms, and DOS at the Fermi level (states/eV spin unit cell) for Fe_3B, Fe_3C and Fe_3N.

	Fe_3B		Fe_3C		Fe_3N	
	Fe (4c)	Fe (8d)	Fe (4c)	Fe (8d)	Fe (4c)	Fe (8d)
Fe $Q^*_\uparrow$ (electron)						
s	0.2367	0.2329	0.2332	0.2316	0.2269	0.2194
p	0.3037	0.3198	0.3504	0.3152	0.3484	0.3180
d	4.5617	4.4453	4.4080	4.3736	4.4115	4.3787
Sum	5.1021	4.9980	4.9616	4.9204	4.9868	4.9161
Fe $Q^*_\downarrow$ (electron)						
s	0.2375	0.2429	0.2498	0.2470	0.2473	0.2380
p	0.3685	0.4019	0.4474	0.3914	0.4570	0.4100
d	2.0391	2.2097	2.2459	2.2872	2.2284	2.2542
Sum	2.6451	2.8545	2.9431	2.9256	2.9327	2.9022
$Q^* = Q^*_\uparrow + Q^*_\downarrow$	7.7473	7.8525	7.9047	7.8460	7.9195	7.8183
$Ms = Q^*_\uparrow - Q^*_\downarrow$	2.4570	2.1435	2.0185	1.9948	2.0541	2.0139
	B $Q^*_\uparrow$ (electron)		C $Q^*_\uparrow$ (electron)		N $Q^*_\uparrow$ (electron)	
s	0.5576		0.7274		0.8453	
p	1.1283		1.4944		1.9306	
Sum	1.6859		2.2218		2.7759	
	$Q^*_\downarrow$ (electron)		$Q^*_\downarrow$ (electron)		$Q^*_\downarrow$ (electron)	
s	0.6205		0.7518		0.8439	
p	1.4179		1.7174		2.0422	
Sum	2.0384		2.4692		2.8861	
$Q^* = Q^*_\uparrow + Q^*_\downarrow$	3.7243		4.6910		5.6620	
$Ms = Q^*_\uparrow - Q^*_\downarrow$	−0.3525		−0.2474		−0.1102	
$N(E_F)_\uparrow(cell)$	4.7885		4.5866		4.9285	
$N(E_F)^\downarrow(cell)$	8.8610		5.3696		8.2713	
$N(E_F)$ *(total)*	13.6495		9.9562		13.1998	

3.3. Magnetic properties of cementite-type Fe_3X (X = B, C, N)

Fig. 5 shows the site- and spin-projected Partial Densities of States (PDOSs) for Fe_3X (X = B, C, N), respectively. For each case, the up and down total densities at each atom are shown separately. From Fig. 5, it can be found that the spin DOSs of Fe atom in Fe_3B, Fe_3C, Fe_3N are different. The effective charges Q^*, their spin components and the spin magnetic moments were calculated according to the Mulliken scheme for each atom in Fe_3X (X = B, C, N) from Fig. 5, which are listed in Table 2.

The average magnetic moments of the Fe_3B, Fe_3C and Fe_3N are 1.5979, 1.4402 and 1.4929 μ_B/atom, respectively. The results of Fe_3C and Fe_3B are similar to that in the literatures [19,20]. The average magnetic moment of cementite–Fe_3N (1.4929 μ_B/atom) is similar to that of ε-Fe_3N (1.44 μ_B/atom) [7]. The differences of Ms between Fe_3X mainly result from that of the spin density difference of Fe and X (X = B, C, N) in the three crystals (see Fig. 5). For cementite-type Fe_3B, the values of Fe Ms are 2.4570 and 2.1435 μ_B for FeI and FeII, respectively. For cementite–Fe_3C, the values of Fe Ms are 2.0185 and 1.9948 μ_B for FeI and FeII, respectively. For cementite-type Fe_3N, the values of Fe Ms are 2.0541 and 2.0139 μ_B for FeI and FeII, respectively. The magnetic character of Fe atom comes from the spin of 3d electrons. The spin density of Fe of Fe_3B is bigger in E_F (the Fermi level) than that of Fe_3C and Fe_3N. The values of atom Ms can be

obtained from the deviation between the up spin occupied state and down spin occupied state. The spin magnetic moment of Fe for Fe_3B is bigger than that for Fe_3N and Fe_3C, so the Ms of Fe_3B is stronger than Fe_3N and Fe_3C. The Ms of Fe_3C is smaller than that of Fe_3N, because the Ms of N (-0.1102 μ_B) is bigger than that of C atom (-0.2474 μ_B) in the crystal. The Fe Ms between two different Fe sites in cementite-type Fe_3X are also different, which indicates that the Fe Ms are sensitive to the local short-range order in the crystals. Similar difference was also found in the literature [19], while the values of moments in Fe are different. The corresponding Q^* for Fe atoms in Fe_3X (X = B, C, N) are similar, but that for B, C and N are different (see Table 2). The corresponding Q^* for N is bigger than that for B and C in Fe_3X (X = B, C, N). This indicates that the ionicity of cementite-type Fe_3N is stronger than Fe_3C and Fe_3B, and that of Fe_3B is weakest in them. This result accords with the DOSs analyses.

4. Conclusion

In summary, a completely theoretical analysis of the structural, electronic and magnetic properties of cementite-type Fe_3X (X = B, C, N) has been presented using first-principles technique. The internal positions of atoms within the unit cell were optimized and the ground state properties such as lattice parameter and the final enthalpy of cementite-type Fe_3X (X = B, C, N) were calculated. The calculated equilibrium structural parameters of Fe_3C and Fe_3B are in agreement with the experimental results. Using the same method the crystal structure of the cementite-type Fe_3N is predicted. From the calculated results, it is confirmed that the bonds of cementite-type Fe_3X (X = B, C, N) are the unusual mixtures of metallicity, covalence, and ionicity. The ionicity of cementite-type Fe_3N is the strongest and the covalence of cementite-type Fe_3B is the strongest in them. The cementite-type Fe_3X (X = B, C, N) are ferromagnetic phases, and the average magnetic moment of cementite-type Fe_3N is predicted as 1.4929 μ_B/atom. The Ms of Fe_3N is bigger than that of Fe_3C, but smaller than that of Fe_3B. Fe moments between two different Fe sites are different in cementite-type Fe_3X (X = B, C, N), which indicates that the Fe moments are sensitive to the local short-range order in the cementite-type crystals.

References

[1] M.J. Baldwin, S.C. Haydon, M.P. Fewell, Surf. Coat. Technol. 97 (1997) 97.
[2] M.I. Ismail, S.S. Iskander, E.B. Saleh, Surf. Technol. 12 (1981) 341–349.
[3] B. Selçuk, R. Ipek, M.B. Karami, et al., J. Mater. Process. Technol. 103 (2000) 310.
[4] S.D. Li, H. Bi, G.Z. Xie, et al., J. Magn. Magn. Mater. 282 (2004) 202.
[5] S. Hirosawa, H. Kanekiyo, T. Miyoshi, et al., J. Alloys Compd. 408–412 (2006) 260.
[6] D. Li, Z.D. Zhang, W.F. Li, et al., J. Magn. Magn. Mater. 307 (2006) 128–133.
[7] A. Houari, S.F. Matar, M.A. Belkhir, M. Nakhl, Phys. Rev. B 75 (2007) 064420.
[8] Matterials Studio, Version 2.1.5. Accelrys Inc., 2002.
[9] W. Kohn, L.J. Sham, Phys.Rev. 140 (1965) A1133.
[10] P. Hohenberg, W. Kohn, Phys.Rev. 136 (1964) B384.
[11] D. Vanderbilt, Phys. Rev. B 41 (1990) 7892.
[12] B. Hammer, L.B. Hansen, J.K. Norskov, Phys. Rev. B 59 (1999) 7413.
[13] H.J. Monkhorst, J.D. Pack, Phys. Rev.B. 13 (1976) 5188.
[14] R. Wyckoff, Crystal Structure. Inter Science, New York, 1964, 564.
[15] F.D. Murnaghan, Proc. Natl. Acad. Sci. U.S.A. 30 (1944) 244.
[16] G. Kresse, D. Joubert, Phys. Rev. B 59 (1999) 1758.
[17] I.G. Wood, L. Vocadlo, K.S. Knight, et al., J. Appl. Crystallogr. 37 (2004) 82.
[18] B. Xiao, J. Feng, C.T. Zhou, J.D. Xing, et al., Chem. Phys. Lett. 459 (2008) 129.
[19] Z.Q. Lv, F.C. Zhang, S.H. Sun, et al., Comput. Mater. Sci. 44 (2008) 690–694.
[20] W.Y. Ching, Y.N. Xu, B.N. Harmon, et al., Phys. Rev. B 42 (1990) 44.